



Information from low-density expendable bathythermograph transects: North Atlantic mean temperature structure and quasi-decadal variability

Robert L. Molinari*

Cooperative Institute for Marine and Atmospheric Studies, Rosenstiel School for Marine and Atmospheric Science, University of Miami, 4600 Rickenbacker Causeway, Miami, FL 33149, United States

National Oceanic and Atmospheric Administration, Ocean and Atmospheric Research, Atlantic Oceanographic and Meteorological Laboratory, Physical Oceanography Division, 4301 Rickenbacker Causeway, Miami, FL 33149, United States

ARTICLE INFO

Article history:

Received 27 April 2010

Received in revised form 15 December 2010

Accepted 19 December 2010

Available online 24 December 2010

ABSTRACT

The 1999 Ocean Observing System conference recommended that the Low density (LD) expendable bathythermograph (XBT) network be discontinued contingent on the completion of studies showing that the global Argo network and/or satellite altimetry can provide equivalent information. Herein, information content in North Atlantic LD lines relative to quasi-decadal variability in upper layer temperature structure is addressed as the first step in achieving this recommendation. Two LD lines are located in the subpolar gyre and support results from previous studies of shorter length that ocean advection and not only air–sea fluxes plays an important role, particularly in the eastern gyre, in determining the characteristics of the water masses transported to the source regions of North Atlantic Deep Water. Several sections cross the Gulf Stream and Labrador Current. They provide evidence to support the hypothesis that changes in the intensity of Labrador Current properties cause meridional motions of the Gulf Stream. Decadal variability in the subtropical gyre of the North Atlantic has been attributed to westward propagation of temperature anomalies by the mean currents and planetary waves. Modeling studies suggest that these signals are dominant in the thermocline at the northern latitudes (order 30°) of the subtropical gyre. Similar calculations from a line crossing the subtropical gyre at these same latitudes shows no indication of westward propagation. Quasi-decadal signals in upper layer temperature are coincident across the entire gyre with some suggestion of eastward motion of temperature anomalies. One line on the southern boundary of the subtropical gyre does include westward signal movement from the eastern boundary. Based on the information content of individual lines, recommendations are made relative to the continuation of specific transects until it has been demonstrated that Argo and satellite altimetry can provide equivalent results.

© 2011 Elsevier Ltd. All rights reserved.

1. Introduction

The expendable bathythermograph (XBT) was initially introduced into the oceanographer's toolbox in the mid-1960s to obtain temperature profiles for naval use (e.g., for rapid regional characterizations of the thermocline depth). It quickly became apparent that the XBT had important scientific applications and was often used in the 1970s and 1980s during limited-region, research cruises. With the advent of the Tropical Ocean Global Atmosphere (TOGA), 1985, and World Ocean Circulation Experiment (WOCE), 1990, programs repeat sampling along transects selected for their scientific value was initiated and the XBT then became a global resource.

Three types of repeat transects were developed for TOGA and WOCE. Low-density (LD) XBT sampling was developed to observe “the large-scale low-frequency modes of climate variability”, Smith et al. (1999). Optimal sampling along the TOGA/WOCE LD lines was established as four XBTs per day (about 170 km between drops from a 15-knot vessel) and 12 times per year. Sampling is primarily from merchant vessels by the ship's crew. The North Atlantic (NA) LD lines addressed in this study are given in Fig. 1. Recently, the LD sampling requirements for many lines have not been met because of the increasing vagaries of the shipping industry (e.g., ships changing routes, ships decommissioned, etc.).

Frequently repeated (FR) and High density (HD) lines were also designed. FR lines are directed at resolving the intense variability of the tropical circulation. Thus, temporal sampling is eighteen times per year, with variable spatial sampling. HD lines are eddy resolving (spatial resolution, 50 km; temporal resolution, 4 times per year) and used to estimate meridional oceanic heat flux through basin-wide, mid-latitude sections (see Baringer and

* Present Address: International CLIVAR Project Office, National Oceanography Center, Southampton, University of Southampton Waterfront Campus, European Way, Southampton, SO14 3ZH, UK. Tel.: +44 23 80 596208; fax: +44 23 80 596204.
E-mail address: Robert.Molinari@noc.soton.ac.uk

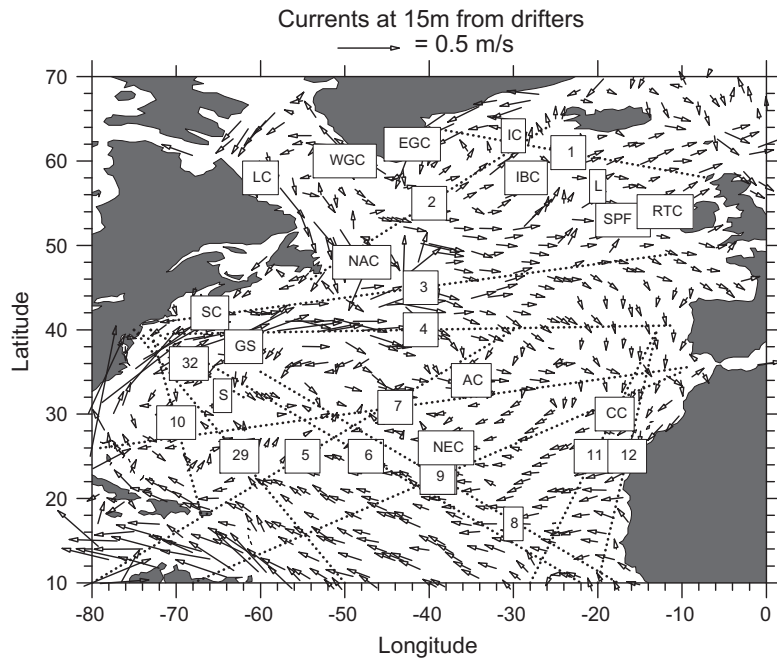


Fig. 1. Low-density transects designated by their WOCE/TOGA line number are superimposed on surface currents derived from the analysis of Lumpkin and Garraffo (2005). Approximate locations of currents crossed by the low-density sections include: LC = Labrador Current; WGC = West Greenland Current; IC = Irminger Current; IBC = Iceland Basin Current; SPF = Subpolar (Arctic) Front; RTC = Rockall Trough Current; NAC = North Atlantic Current; SC = Slope Current; GS = Gulf Stream; AC = Azores Current; CC = Canary Current; and NEC = North Equatorial Current. The letters S and L give the locations of Stations S and Lima.

Garzoli, 2007, for example). Data from FR and HD lines will be used in the present study when they overlap LD lines.

In view of the greater spatial and temporal coverage provided by the Argo array (Gould et al., 2004) and satellites, the need for maintaining the LD network was raised by Smith et al. (1999). They recommended that LD sampling be discontinued *contingent* on the completion of studies demonstrating the ability of the former systems to provide information comparable to the latter. The present study represents an initial step in ensuring this capability, that is, identifying important signals that can be resolved by LD observations.

The information content from LD lines ranges widely on both spatial and temporal scales and it was thus necessary to select one issue of scientific importance in a region of adequate LD coverage. Quasi-decadal time-scale variability in the North Atlantic (NA) has gained recent attention because of its potential relevance to global climate and the need to distinguish natural from anthropogenic climate variability. Thus, the present effort will concentrate on quasi-decadal variability of upper layer temperature in the subtropical and subpolar NA. Recommendations on the future of the LD network will complete the paper.

2. Background

2.1. The XBT

A very brief description of the XBT is provided to identify how temperature and depth pairs are observed. The Sippican Corporation (now Lockheed Martin Sippican) has manufactured the majority of XBTs. The initial Sippican XBT probe, the T-4, was designed to sample to a maximum depth of 450 m. Two deeper reaching XBTs, the T-7 and the Deep Blue, were introduced in the mid-1970s. Both probes were designed to sample to 750 m. Sippican licensed the manufacture of XBT probes to Tsurumi Seiki Co., Ltd in the early 1970s. For purposes of the present study probes manufactured by either company will be considered to have similar properties.

The XBT measures temperature with a thermister placed in the nose of the probe. The manufacturer's stated accuracy is ± 0.15 °C for T-4 and T-7/Deep Blue probes (Sippican, 1983). The XBT does not measure depth directly. Depth is inferred from an empirically determined Fall Rate Equation (FRE), which estimates depth in terms of time from the probe entering the water. Sippican (1983) specified depth uncertainty as $\pm 2\%$ or ± 5 m whichever is greater.

2.2. Data and analyses

Data sources, with an emphasis on meta-data, and analytical methods are now described. The XBT data were obtained from the National Oceanographic Data Center (NODC) of the National Oceanic and Atmospheric Administration. The data set used herein extends from January 1967 through December 2004. The data have been edited and duplicates removed. Flags accompanying the profiles indicate the quality of an observation and range from 1, a good profile to 4, an erroneous profile. Only profiles with flags of 1 or 2 (probably good) are used in this paper.

Other meta-data are provided with the temperature-depth pairs from individual profiles. Unfortunately, meta-data provided are often incomplete or erroneous. For instance, as will be described in more detail, the manufacturer's FRE is incorrect and corrections have been developed. A small percentage of the data includes no information on whether or not a correction was applied. These 'unknown' profiles are not used in the analyses. Similarly, the type of probe is frequently not given, information required as different corrections have been estimated for shallow and deep XBTs.

In this study, sea-surface temperature (SST) and the depth-averaged temperature of the upper 400 m (T400) are used to address upper layer decadal variability. T400 was selected, as particularly prior to 1970, a large number of shallow XBTs did not reach 450 m. Use of deep XBTs did not become prevalent until the 1990s (Wijffels et al., 2008, hereinafter W08).

It is recognized that XBT data are not optimal for studying SST over large areas, primarily because of limited coverage when

compared to satellites. However, LD XBT data do possess some positive attributes for studying SST collected along repeated transects and research cruises including: (1) the same sensor is used for data collection, (2) SST is measured at approximately the same depth (~3 m) compared to the variable depths of ship intake observations, (3) XBT SST values were frequently verified by bucket temperatures during early research cruises, and (4) data collected along well-sampled lines give sufficient coverage to resolve SST variability.

Data were averaged onto an along-line grid to generate time-distance plots (TDP) of SST and T400. LD lines are seldom exactly repeated from crossing to crossing because of weather, changes in ports of call, etc. In addition, meta-data identifying the line on which an XBT was deployed are in general not provided with the profile. Placing XBTs on the specific line occupied is a significant effort and beyond the scope of this study. For this reason, data within a swath, $\pm 1.5^\circ$ from the ideal section are used to generate the TDPs.

The 3° -band was used after some testing with other widths and along the lines selected was judged to be adequately narrow to avoid aliasing by surrounding temperature gradients. Particularly prior to TOGA and WOCE, XBTs not taken along a specific line but within $\pm 1.5^\circ$ of the line are added to the data used to generate section products. Thus, most TDPs include more data than would be used if only observations from occupations of specific LD transects were employed.

To highlight quasi-decadal variability in the TDPs, linear trends were removed from all time series. A least squares fitting routine was used to compute the trends. Trends are computed from the observations available at each data point, thus the length of time over which trends are computed varies.

The characteristics of the distance axis are dependent on the orientation and length of the line. LD lines oriented primarily in the east–west direction use longitude as the distance axis and north–south lines, latitude. The mapping routine used to generate TDPs limits the number of grid points allowed. Thus, the averaging interval along the distance axis varies depending on the length of the line being considered and ranges from 0.5° for shorter lines to 2° for longer lines.

The temporal averaging period was two months. Bimonthly anomalies were computed relative to the record length average. W08 note that several years typically passed after purchase of a probe before an XBT is used. Thus, they average data with a 2-year running mean. Herein, a somewhat more conservative 3-year running average is used to generate the TDPs.

The mapping routine used to generate TDPs can mask areas with little or no data. Areas along the boundaries of the grid without data are automatically blanked. Those points within the grid without data are interpolated using the number of surrounding grid points requiring data (usually 2 along each axis) and the minimum number of data points desired in each quadrangle (typically 4).

Average vertical sections were also generated for each line using the same editing, orientation and grid spacing conventions just described. When placing the XBT measurements on either a vertical or a time-distance grid, a 1.5 for SST and 2 for T400 standard deviation test was applied at each grid quadrangle to remove any questionable data that passed the data center's edit. The choice of standard deviation was made assuming that SST fields are generally noisier than T400 fields.

2.3. Fall Rate Equation

Depth biases in the XBT data are now described in order to provide uncertainty estimates for the analyses. As described previously, the depth of an XBT temperature observation is not

measured directly but is estimated using a FRE. Depth (Z_{XBT}) is determined from the relation

$$Z_{\text{XBT}} = a * t - b * t^2 \quad (1)$$

t is time from when the XBT enters the water, a is a coefficient dependent on the hydrodynamic characteristics of the probe in water, and b is a coefficient dependent on the changing mass of the probe caused by unreeling of wire as it falls through a depth dependent density column.

Shortly after the introduction of XBTs, it was recognized that depths calculated using the coefficients provided by the manufacturer resulted in uncertainties greater than specified. However, these early studies were based on only limited data (i.e., typically one or two cruises comparing XBT depths with more accurate Conductivity-Depth-Temperature (CTD) units and/or reversing thermometers placed on Nansen Bottles). In addition to fall rate errors, temperature biases have also been identified (e.g., Gouretski and Koltermann, 2007; Levitus et al., 2009).

Hanawa et al. (1995), H95, confirmed earlier studies, which found that the manufacturer's FRE underestimated the actual fall rate of the XBT. This error placed the XBT at a shallower depth than its true deeper depth resulting in a lower than actual temperature recorded by the probe at the given depth. Thus, a cold bias for the uncorrected temperature observations results for most profiles.

Several approaches have been developed to correct biases in XBT depths and/or temperatures. H95 directly compared XBT and CTD/bottle profiles co-located in both time and space and collected between 1985 and 1992 (i.e., a short temporal record). They computed new coefficients for each instrument pair by aligning temperature gradients such that "bias-like temperature errors can be eliminated" (i.e., potential temperature biases were not addressed). They derived mean coefficients by averaging almost 300 independent estimates.

Instead of using Eq. (1) with new coefficients, H95 recommended implementation of a simplified correction for the Sippican and Tsurumi probes given by,

$$Z_{\text{Hanawa}} = 1.0336 * Z_{\text{XBT}} \quad (2)$$

where Z_{XBT} is given by (1). They estimate a mean depth error using (2) of ± 1 m.

More recent studies such as those by Gouretski and Koltermann (2007), Levitus et al. (2009), Ishii and Kimoto (2009) and W08 employed more data and used different data and methods to develop more accurate corrections for XBT temperature and/or depth biases. The W08 method for correcting depth biases will be used in the present study (i.e., an explicit temperature correction will not be applied) for reasons to be given shortly. W08 derived a probe and time dependent correction by comparing XBT profiles to climatological fields that is given by:

$$Z_{\text{Wijffels}} = [1 - r_{i=1,2}(t)] * Z_{\text{Hanawa}} \quad (3)$$

Z_{Hanawa} is given by (2) (i.e., the H95 correction is first applied then the W08 correction), t is the year of the observation, and the $r_i(t)$ s are the different correction coefficients for shallow and deep probes. W08 estimate errors for both the shallow and deep coefficients of less than 2%.

In an attempt to apply the appropriate correction when the probe type is not given in the meta-data, profiles that extended to or less than 550 m were considered to be T-4 probes, while those that extended to greater than 550 m, T7/Deep Blue. W08 inferred that the source of uncertainty probably resulted from subtle time dependent manufacturing changes. They went onto conclude that FRE errors are most likely the largest source of biases in XBT data.

Support for the W08 correction is found in Levitus et al. (2009) who provide a mean global section of differences between W08 corrected temperatures and those from a climatology that does not

include XBT data. Below 100 m, absolute differences are less than 0.1 °C. Domingues et al. (2008) compute global ocean heat content for the upper 700 m using the W08 corrections. The largest difference between corrected and uncorrected estimates of heat content are found in 1975 and equates to a temperature difference of about 0.1 °C. Thus both studies produce similar average uncertainties.

Levitus et al. (2009) note that differences in the magnitude of temperature errors can be caused by regionally different vertical temperature structure. Two stations, one in the subtropical and the other in the subpolar NA, are used to address this issue. Quasi-monthly hydrographic data have been collected at Hydrostation S (Phillips and Joyce, 2007) located near Bermuda at a nominal position of 32°10'N, 64°30'W (Fig. 1). This station is close to several XBT lines (Fig. 1). Station S data collected between 1967 and 1989 were retrieved for the present study.

Vertical time series sections of temperature anomaly have been generated using both W08 corrected XBT depths and the hydrographic data from Station S (not shown). Data within 5-degrees of the mean position of Station S were used to generate the XBT record. The anomalies are computed relative to the mean annual cycle of the two independent 1967–1989 time series.

Largest differences between the sections appear above 100 m centered at about 1973 and 1979 (Fig. 2). The Station S anomaly plot (not shown) includes large negative temperature anomalies at these times not found in the XBT plot. These large differences have several potential causes including: (1) the limited sampling at Station S (an average of 16 stations per year) compared to the larger XBT database (an average of 277 probes per year); (2) different positions for the mean locations of the two data sets; and/or (3) different temporal coverage of the two data sets. The root mean

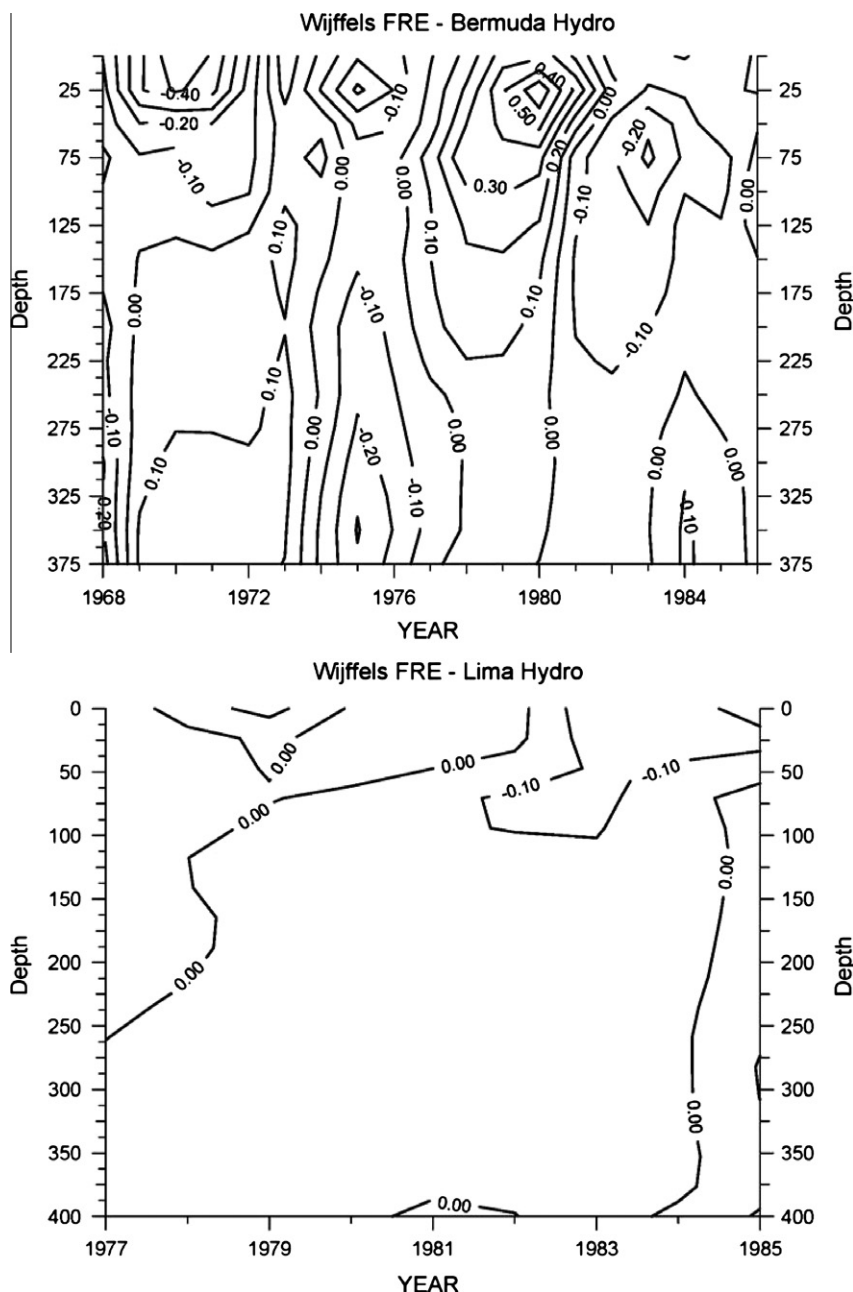


Fig. 2. Time versus depth plots of temperature anomaly differences (°C) between the hydrographic and XBT time series taken at Station S (upper panel) and Station Lima (lower panel). Contour interval is 0.1 °C.

square difference between the two anomaly plots for depths greater than 100 m is 0.11 °C.

Ocean weather ship Lima is located in the subpolar Atlantic at a nominal position of 57°N, 20°W (Fig. 1). Calculations similar to those performed for the Bermuda station were applied to the shorter Lima record. The mean temperature time series displays a more barotropic temperature structure than observed at Bermuda (not shown). The total water column average difference below 100 m (Fig. 2) between the XBT and hydrographic temperature anomaly sections is less at Lima, 0.05 °C, than at Station S, 0.11 °C.

The W08 correction is applied to the entire profile. Both the historical studies described and the calculations performed suggest 0.2 °C as a conservative estimate for the uncertainties in temperature used in this paper. This estimate is close to the manufacturer's uncertainty for temperature, 0.15 °C.

2.4. Scientific issues

The major atmospheric and oceanic scientific issues related to quasi-decadal variability in upper Atlantic temperature characteristics are now described. The North Atlantic Oscillation (NAO) is an atmospheric teleconnection pattern (Wallace and Gutzler, 1981), which is characterized by shifts in sea level pressure between the polar and subtropical NA. The NAO index has been defined by the pressure difference between meteorological stations in Iceland and the Azores (Hurrell, 1995). Encompassing the NA westerlies, positive NAO indices are correlated with increased westerlies and negative NAO indices with weakened westerlies. In addition, a similar relation is observed between the NAO and the Trade Winds. Hurrell et al. (2003) provide a detailed review of the mean and time dependent structure of the NAO.

A repeated theme in previous studies of NA variability is that on decadal time scales the NAO imprints SST and subsurface variability in the basin. However, the mechanisms responsible for this role

remain controversial (see Visbeck et al., 2003). A first-order question involves the relative importance of local (i.e., air–sea fluxes) versus remote (i.e., ocean circulation) forcing. Hurrell et al. (2003) state a possible reason for this question, “There is no unique way to define the spatial structure of the NAO, or thus its temporal evolution”.

3. Results

3.1. The LD network and average surface currents of the North Atlantic

Fig. 1 shows the NA LD transects addressed herein superimposed on the distribution of total average surface currents derived from satellite-tracked surface drifters (Lumpkin and Garraffo, 2005). LD lines north of 20°N will be studied. This depiction of surface currents and those from other studies will be used in conjunction with isotherm slopes and near surface temperatures to confirm flow directions.

3.2. Individual lines

Vertical sections of mean temperature are used to identify the currents crossed by the transects. Although neither shown nor discussed because of the emphasis on quasi-decadal signals, other properties such as standard deviations, properties of the annual and semi-annual harmonics, etc. can be calculated from these data. This information can be used in comparisons of numerical model and XBT ocean characterizations.

The slope of the isotherms only signifies the sense of the vertical geostrophic current shear. Thus, comparisons are made with several drifter representations of surface flow particularly those of Flatau et al. (2003), hereafter F03, and those shown in Fig. 1 to verify the inferences about flow direction derived from geostrophy. F03 subtracted Ekman drift estimates from total float velocity to

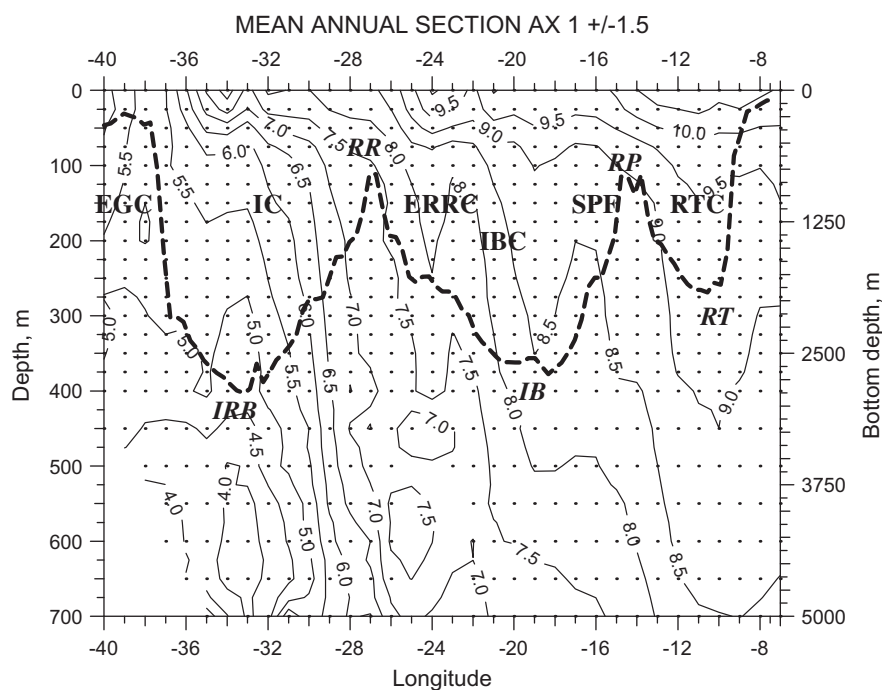


Fig. 3. Average temperature section (°C) for section AX1 (see Fig. 1 for location of section). Thick dashed line represents bottom topography along the line. X-axis is longitude and Y-axis on left side is depth for temperature section in meters and on right side bottom depth in meters. Horizontal grid spacing is 1° and vertical spacing 25 m above 400 m and 50 m below 400 m. Approximate positions of the currents crossed by AX1 include: EGC = East Greenland Current; IC = Irminger Current; IBC = Iceland Basin Current, SPF = Subpolar (Arctic) Front; RTC = Rockall Trough Current. Approximate positions of topographic features crossed by AX1 include: IRB = Irminger Basin, RR = Reykjanes Ridge; IB = Iceland Basin; RP = Rockall Plateau; and RT = Rockall Trough.

generate geostrophic surface currents. Fig. 1 gives the total surface current derived from drifter data. F03 find that in most regions of the Subpolar Gyre (SPG), the differences between the two representations are not significant.

3.2.1. AX1

This approximately zonal transect extends from Ireland/Scotland to Greenland (Fig. 1), crossing flow into and out of the source regions for components of North Atlantic Deep Water (NADW). The AX1 ensemble average vertical temperature section is given in Fig. 3. Isotherms that slope downward from west to east are indicative of northward geostrophic shear and those from east to west, southward shear.

AX1 crosses four northward flowing currents. At 33°W, along the western side of Reykjanes Ridge, isotherm slope, Fig. 3, is indicative of the northward flowing Irminger Current. This current occu-

pies a similar position in both the F03 and Fig. 1 surface current maps.

The Iceland Basin Current is one of the few flows in the subpolar Atlantic that is not constrained to flow along a continental slope. Between about 22°W and 19°W, both the isotherm slopes (Fig. 3) and the current distributions in F03 and Fig. 1 indicate that this current flows to the north through the center of the Iceland Basin. The surface drifter representations of the Iceland Basin Current suggest a more easterly than northerly component as it crosses AX1.

Brambilla and Talley (2008), BT08, provide a schematic diagram of the surface currents in the eastern SPG derived from drifters and hydrography. The Subpolar Front flows north along the western side of the Rockall Trough consistent with the slope of the isotherms between 17°W and 15°W. BT08 show that the North Atlantic Current (NAC) (Fig. 1) splits at about 55°N, 27°W to form the

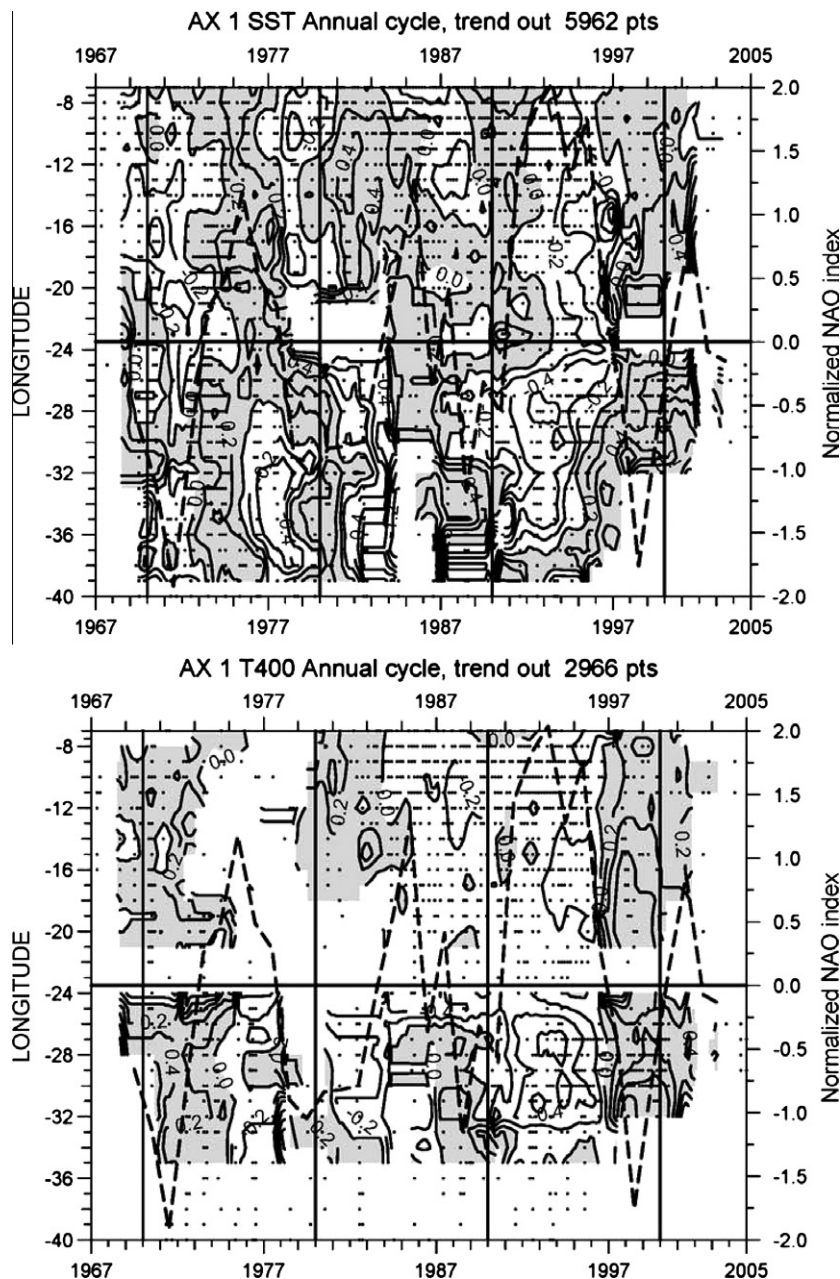


Fig. 4. Upper panel: Sea-surface temperature, °C. Lower panel: Depth-averaged temperature of the upper 400 m, °C. For both panels contours plotted on a 2 month by 1° of longitude grid. X-axis is time in years, Y-axis, left side direction, right side normalized NAO index. NAO index time series given by thick dashed line. Data points indicated by dots. Total number of points used to generate the time series is given in upper title.

Iceland Basin Current and the Subpolar Front. This connectivity with the NAC is responsible for surface temperatures greater than 9.5 °C east of about 25°W (Fig. 3).

Highest near surface temperatures along AX1 are observed between 15°W and 7°W (Fig. 3). The isotherm slope between 16°W and 11°W is indicative of northward flow in the Rockall Trough (Fig. 1), hereinafter the Rockall Trough Current. This flow is also an extension of the NAC (BT08, for instance) explaining the higher temperatures.

Southward flow occurs at the extreme western end of AX1 where because of seasonal ice coverage sampling is primarily during ice-free months (e.g., Krauss, 1995). The isotherm slope (Fig. 3) and a schematic diagram generated by Pickart et al. (2005) show AX1 is located within the southward flowing East Greenland Coastal Current. The combined East Greenland Current and Irminger Current, indistinguishable in the temperature section, are shown by the isotherm slope to continue flowing south to about 38°W as in Pickart et al. (2005).

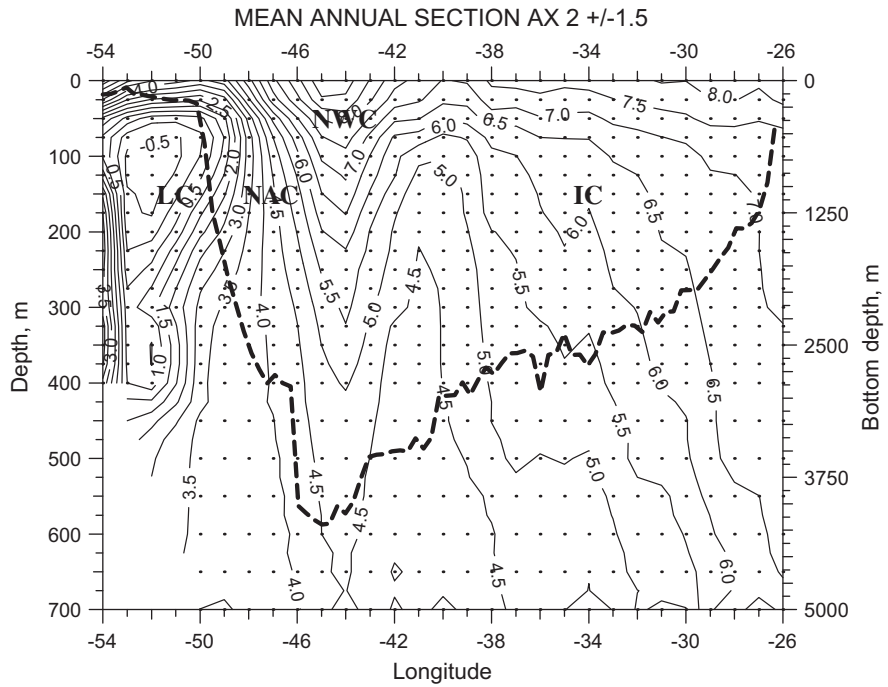


Fig. 5. Same as Fig. 3, except for AX2: LC = Labrador Current, NAC = North Atlantic Current, NWC = Northwest Corner; and IC = Irminger Current.

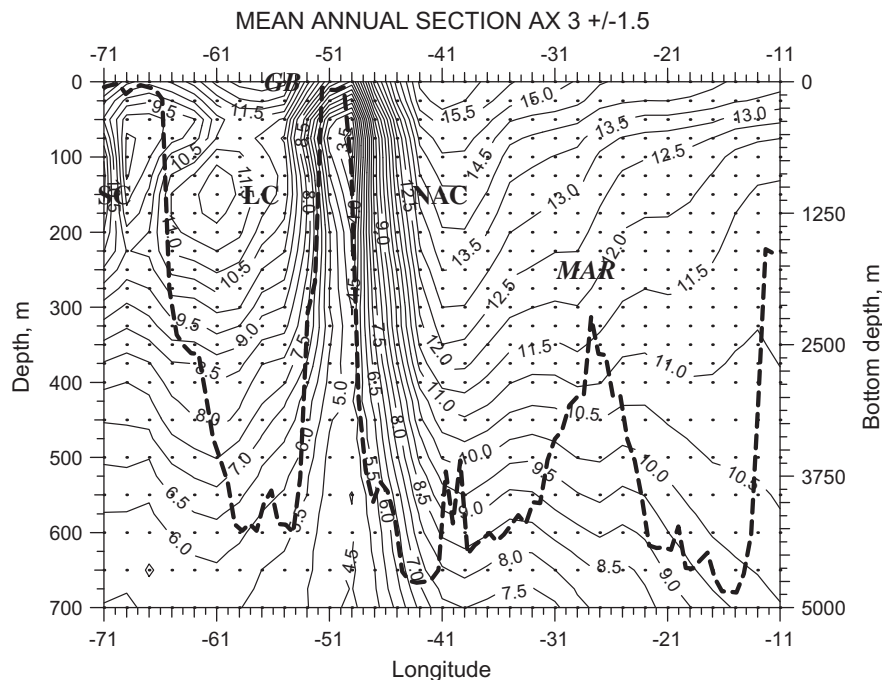


Fig. 6. Same as Fig. 3, except for AX3: SC = Slope Current; LC = Labrador Current; NAC = North Atlantic Current; GB = Grand Banks; and MAR = Mid-Atlantic Ridge.

On the eastern flank of the Reykjanes Ridge, BT08 depict a southwestward flowing East Reykjanes Ridge Current between about 64°N and 59°N. The subsampling used to generate Fig. 1 fails to resolve this narrow flow. However, when all vectors are plotted (not shown), this southerly current is apparent. Southerly geostrophic shear is consistent with the slope of the isotherms below 100 m between 24°W and 23°W (Fig. 3).

The dominant resolvable signal in the SST and T400 TDPs is associated with the winter 1995/1996 reversal in NAO index (Fig. 4). F03 used surface drifters, SST and surface heat flux data to study this period of the weakening of the SPG (e.g., Häkkinen and Rhines, 2004). F03 observe intensified northeast flow; a westward retraction of the Subpolar Front, a change from negative to positive SST anomalies and eastward propagating signals associated with this event.

The change in the sign of SST and T400 is observed along the entire length of AX1 where data are available (Fig. 4) coincident with

the retraction of the Subpolar Front across the entire eastern SPG (e.g., F03). There is the suggestion of eastward propagation of anomalies in the SST plots but not in the T400 record. Prior to the mid-1990s event, the data are too sparse and noisy to discern other signals in the SST time series west of about 20°W (Fig. 4).

East of about 20°W there is a quasi-decadal signal in SST characterized by changes in the sign of SST anomaly coincident with extremes in the NAO. For instance, in the Rockall Plateau and Trough region (Fig. 3), the 1971.5, 1979.5 and 1988.5 minima in NAO index are approximately coincident with changes in SST anomaly from positive to negative (Fig. 4). Conversely, changes in SST anomaly from positive to negative occur with the extreme positive NAOs of 1974.5 and 1985.5.

The T400 data are more limited than the SST data (Fig. 4). However, along the extreme eastern boundary of AX1 there is a period of negative anomaly from about 1984 through 1997, except for the small area of positive anomaly between 1990 and 1993. This long

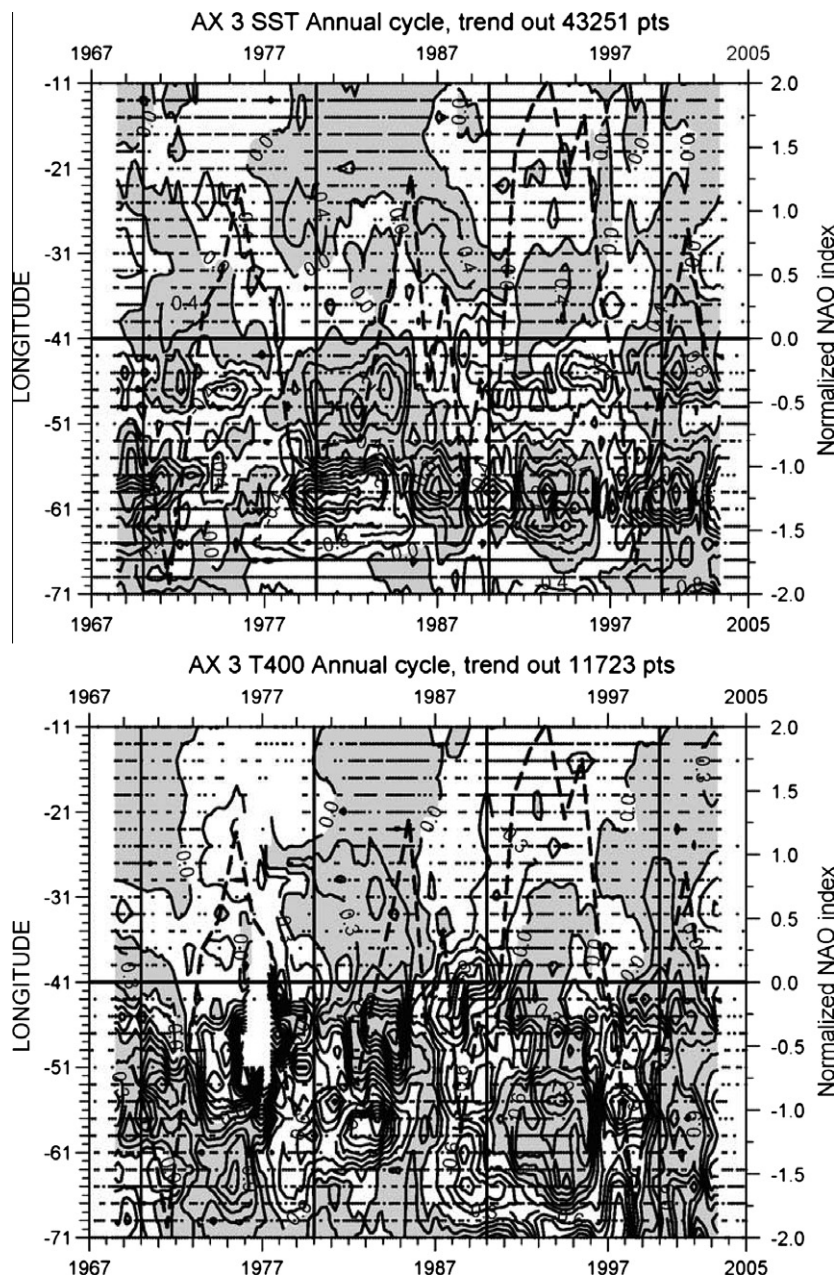


Fig. 7. Same as Fig. 4, except for AX3 and contour interval of 0.4 °C for both panels.

temporal extent of the T400 anomaly is consistent with the sea surface height signal described by Häkkinen and Rhines (2004) in a study of the 1990s weakening of the SPG.

3.2.2. AX2

This transect extends from Newfoundland to Iceland (Fig. 1). Reverdin et al. (1999), R99, reported on a 5-year (1993–1998) occupation of AX2 during WOCE. They note that two distinct lines were occupied one northwest of the other. Averaging data from both lines could produce aliased temperature structures, so they used only data from the southeast line. Using a ± 1.5 swath around the mean position of AX2 has the effect of using data primarily from the southeast occupations of the transect.

R99 generated a mean annual temperature section from the 5-year occupation of AX2. A mean section from data collected along AX2 from 1967 through 2004 is given in Fig. 5. The average sections are similar because of the predominance of data collected during the 5-year WOCE period. Thus only a brief description of the mean section from the longer record is given.

Proceeding eastward from the boundary, AX2 crosses the southward flowing Labrador Current indicated by isotherms below about 75 m sloping downward to the west in the mean temperature section (Fig. 5). The Labrador Current extends to about 48°W . As in R99, the Labrador Current is characterized by a temperature minimum at about 80 m. R99 indicate that the minimum represents the deepest depth of the winter mixed layer.

A band of higher temperatures is observed between 48°W and 42°W (Fig. 5) representing “the northwest corner extension of the North Atlantic Current”, R99 (i.e., where the NAC retroflects from northerly to easterly flow). The isotherm slope beginning at about 38°W indicates that the AX2 is crossing the northward flowing Irminger Current. The isotherms shoal below 100 m between about 36.5°W and 34.5°W . The isotherm slope to the end of the section is again consistent with the section continuing to cross the Irminger Current. Possibly, there are two distinct bands of

the Irminger Current and/or temporal shifts in the flow that AX2 crosses.

The AX2 SST and T400 anomaly records show the same mid-1990s signal as observed in the AX1 time series (not shown). That is, after the winter of 1995/1996 change from high to low NAO index, SST and T400 values transition from negative to positive anomalies. Previous to this event, SST and T400 data are sparser and noisier along AX2 precluding any definitive statements on possible signals.

3.2.3. AX3 and AX4

AX3 extends from New York to Southwestern England and AX4 from New York to Europe along approximately 40°W , Fig. 1. AX4 is located closer to the axis of the Gulf Stream (GS) than AX3 (Fig. 1) but features are comparable. In addition, SST and T400 variability along the two sections is similar, particularly along their western boundaries. AX3, unlike AX4, crosses the Slope Current and will be addressed here.

From 71°W to 67°W , currents in Fig. 1 and from Fratantoni (2001) indicate that AX3 is crossing the westward flowing Slope Current. At this location, AX3 crosses a subsurface temperature minimum centered at about 75 m (Fig. 6), as crossed by AX2 farther to the east in the Labrador Current (Fig. 5). Thus, the Slope Current is transporting properties from the Labrador Sea to the western slope north of the GS as observed in other studies (e.g. Greene and Pershing, 2003).

Total surface current representations from Fig. 1 and Fratantoni (2001) indicate that AX3 is located to the north of the GS axis between about 65°W and 55°W . Isotherm slope between 55°W and 51°W (Fig. 6), Fig. 1, Fratantoni (2001) and the temperature minimum at 75 m all indicate that AX3 is now crossing the southward extension of the Labrador Current.

On the eastern side of the Grand Banks, from 50°W to 39°W , isotherms slope dramatically downward to the east (Fig. 6), placing AX3 in the NAC. From 41°W to 28°W (the crest of the Mid-Atlantic Ridge, MAR), AX3 is located in the GS extension (Fig. 1). From the

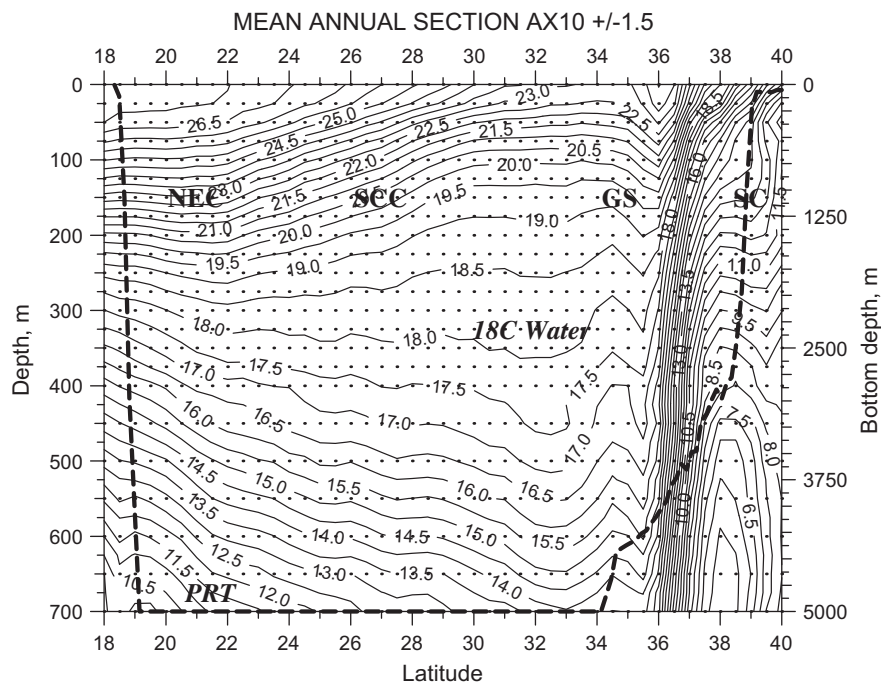


Fig. 8. Same as Fig. 3, except for AX10 and NEC = North Equatorial Current, SCC = Subtropical Countercurrent, 18 C water = the 18 °C mode water, GS = Gulf Stream, SC = Slope Current, and PRT = Puerto Rico Trench. Bottom depths greater than 5000 m are not shown.

crest of the MAR at 28°W to 11°W, isotherms slope in different directions above and below 400 m (Fig. 6). In this band, AX3 is crossing the Canary Current, Fig. 1, i.e., the eastern boundary of the STG.

West of 55°W/53°W, the large anomalies in SST and T400 (Fig. 7) are characteristic of the meridional shifts in GS position as described in Joyce et al. (2000) and Molinari (2004), for example. Specifically, the GS crosses AX3 between about 67°W and 55°W with a quasi-decadal signal as found in these earlier studies. The large variability in SST between 53°W and 40°W encompasses the portion of AX3 crossing the Labrador Current and the region where the GS becomes the NAC (Fig. 1).

However, the signatures of the SST variability in the extension of the Labrador Current and the NAC are different than that observed to the west in the migrating GS. Variability in the former features has a longer period (multidecadal) than the quasi-decadal period in GS movement (Fig. 7). The T400 TDP exhibits similar

increased amplitude anomalies east of the GS shifts. However, particularly where data are plentiful, these T400 anomalies are often in-phase with GS meanders (e.g., 1987–1993, 1993–1996, 1996–1999, 1999 to the end of the record). Thus, different processes are active at the surface and deeper in the water column.

3.2.4. AX10, AX29 and AX32

AX10 extends from New York to Puerto Rico, AX29 from New York to east of South America and AX32 from New York to Bermuda (Fig. 1). Thus, at their northern ends the three sections are approximately coincident. At its Bermuda end AX32 is about 400 km east of AX10. AX29 is located between these two other sections. Because of their proximity to AX10, the details of the AX29 and AX32 anomalies are similar to those along the westernmost transect. These lines will not be discussed further.

AX10 crosses the Slope Current between 39°N and 40°N as indicated by the isotherm slopes (Fig. 8) and total surface currents

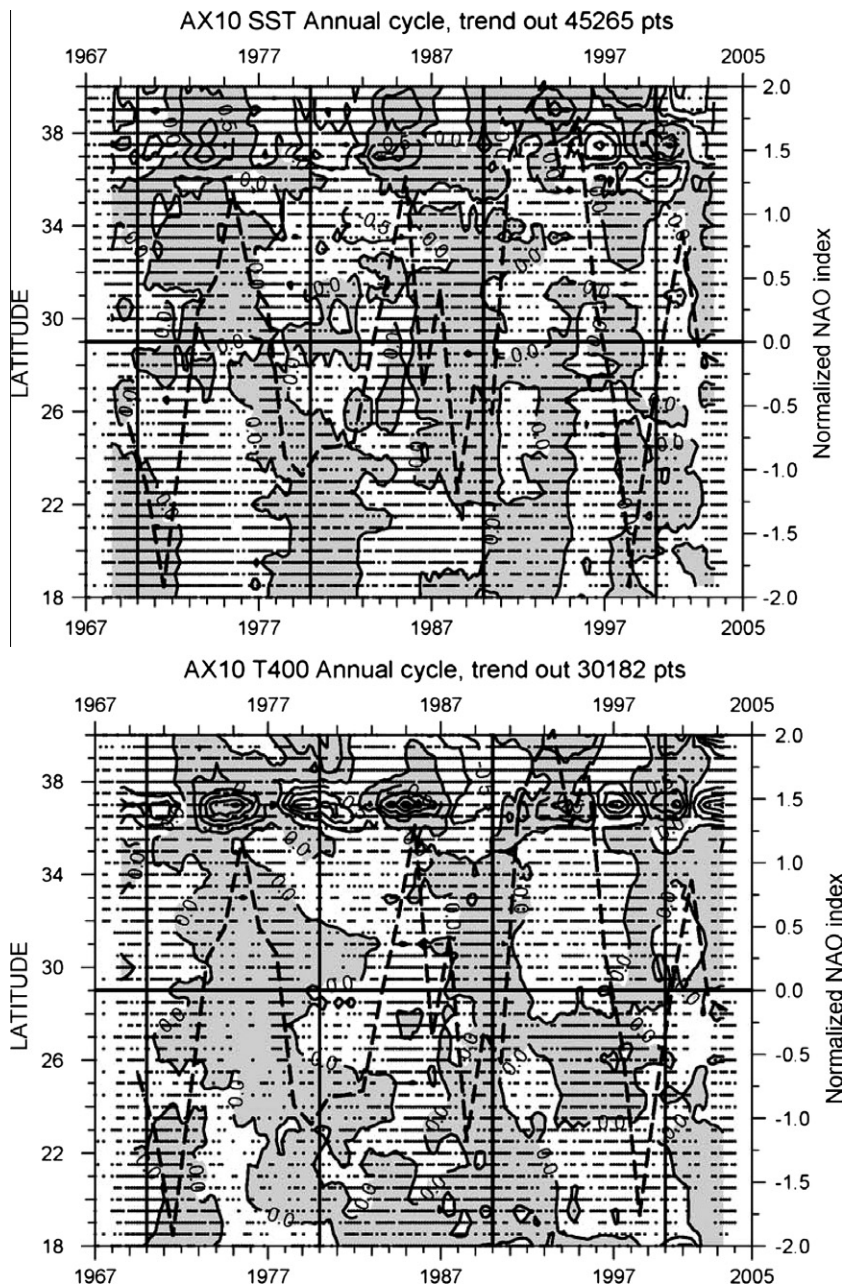


Fig. 9. Same as Fig. 4, except for AX10 and contour interval of 0.5 °C for both panels.

(Fig. 1). Dynamic height topographies from the western STG show a “C”-structure in the western Sargasso Sea (e.g., Stommel et al., 1978 and Tsuchiya, 1985). AX10 crosses this feature, which extends meridionally from the GS to the North Equatorial Current and zonally from the western boundary to about 60°W.

Along AX10, the northern limb of the C-structure is the GS, represented by the intense temperature gradients located between about 36°N and 38°N (Fig. 8). AX10 crosses the southern side of

the northern limb of the C-structure between about 30°N and 33°N. The westward flow of this limb is consistent with the slope of the isotherms in the main thermocline and represents the recirculation gyre south of the GS, Fig. 1.

At the surface between 26°N and 30°N, more intense temperature gradients are indicative of the Subtropical Frontal Zone (Fig. 8) as shown in Halliwell et al. (1994). Although the isotherm slopes indicate opposing geostrophic shears with depth in this band, the

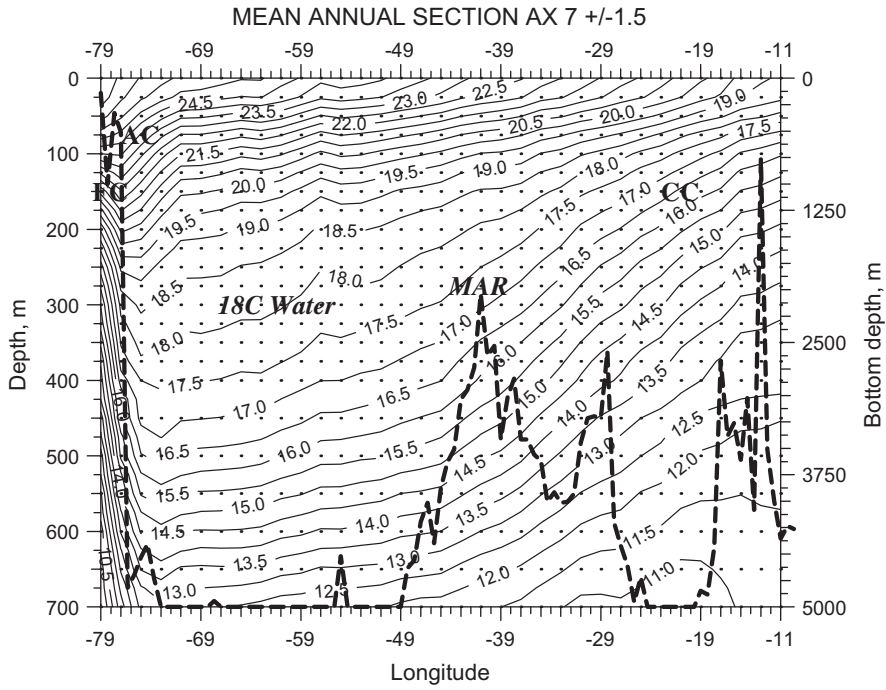


Fig. 10. Same as Fig. 3, except for AX7 and FC = Florida Current, AC = Antilles Current, 18 °C Water = the 18 °C mode water, CC = Canary Current, and MAR = Mid-Atlantic Ridge. Bottom depths greater than 5000 m are not shown.

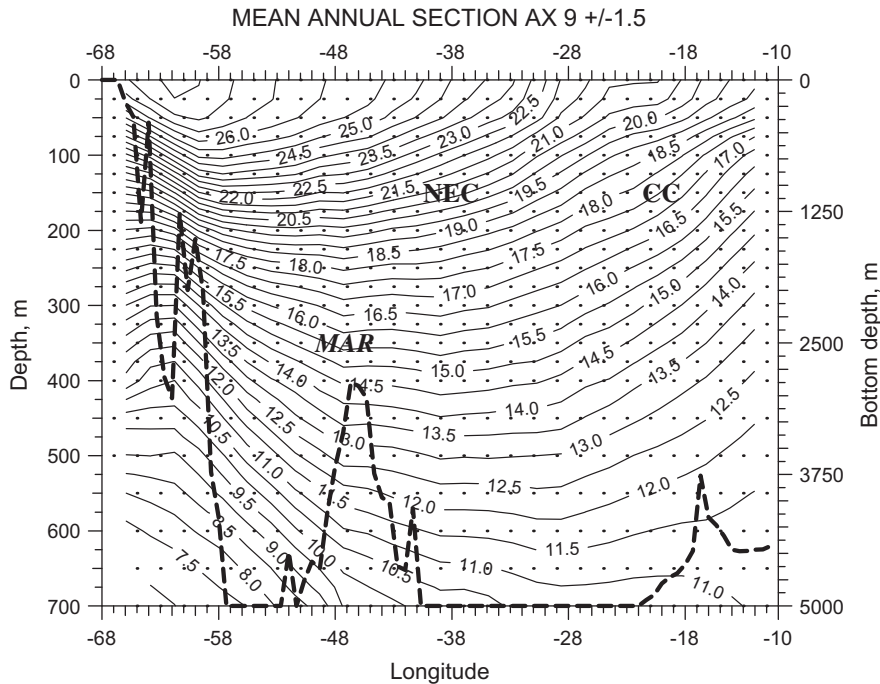


Fig. 11. Same as Fig. 3, except for AX9 and NEC = North Equatorial Current, CC = Canary Current, and MAR = Mid-Atlantic Ridge. Bottom depths greater than 5000 m are not shown.

directly observed surface currents in Fig. 1 are to the east consistent with the direction of the Subtropical Countercurrent, Halliwell et al. (1994), for example. South of this flow, the North Equatorial Current is located adjacent to the boundary in a band where the permanent thermocline slopes upward to the boundary and the seasonal thermocline is approximately horizontal (Fig. 8).

Molinari (2004) found north–south quasi-decadal migrations of the GS along AX10 with a range of about 100 km in a time series of temperature at 150 m. These migrations are evident in the SST and T400 TDPs of Fig. 9 as approximately shaped ‘bulls-eyes’ with a period of 8–10 years. Joyce et al. (2000) observed a similar range of GS movement over a 1000 km band somewhat to the east of AX10. The migrations in Molinari (2004) lagged peaks in the NAO-index by 1-year, in contrast to the in-phase relation found by Joyce et al. (2000).

The SST time series within the latitudinal range of the southern limb of the northern C-feature, 30–36°N (i.e., the southern recircu-

lation gyre of the GS) is noisy because of the proximity to the GS. However, both the SST and T400 series display a slightly longer period than the GS signal, which is more apparent in the latter record (Fig. 9) and suggests that different processes are causing the signals within and to the south of the GS.

The SST signals in the 30–36°N band and the southern limbs of the C-feature, including the North Equatorial Current (25°N to the southern boundary) are approximately out of phase (Fig. 9). In the band south of 25°N, the SST signal is approximately decadal. However, there is no obvious relation to the NAO (Fig. 9).

From about 1973 to 1994, T400 anomalies generally extend from the GS to just north of the North Equatorial Current, 22°N, with a slightly longer than decadal period (Fig. 9), suggesting that the STG is weakening (cold anomalies) or strengthening (warm anomalies) simultaneously between these two currents. After 1994, a tripole like structure is observed in the T400 anomalies.

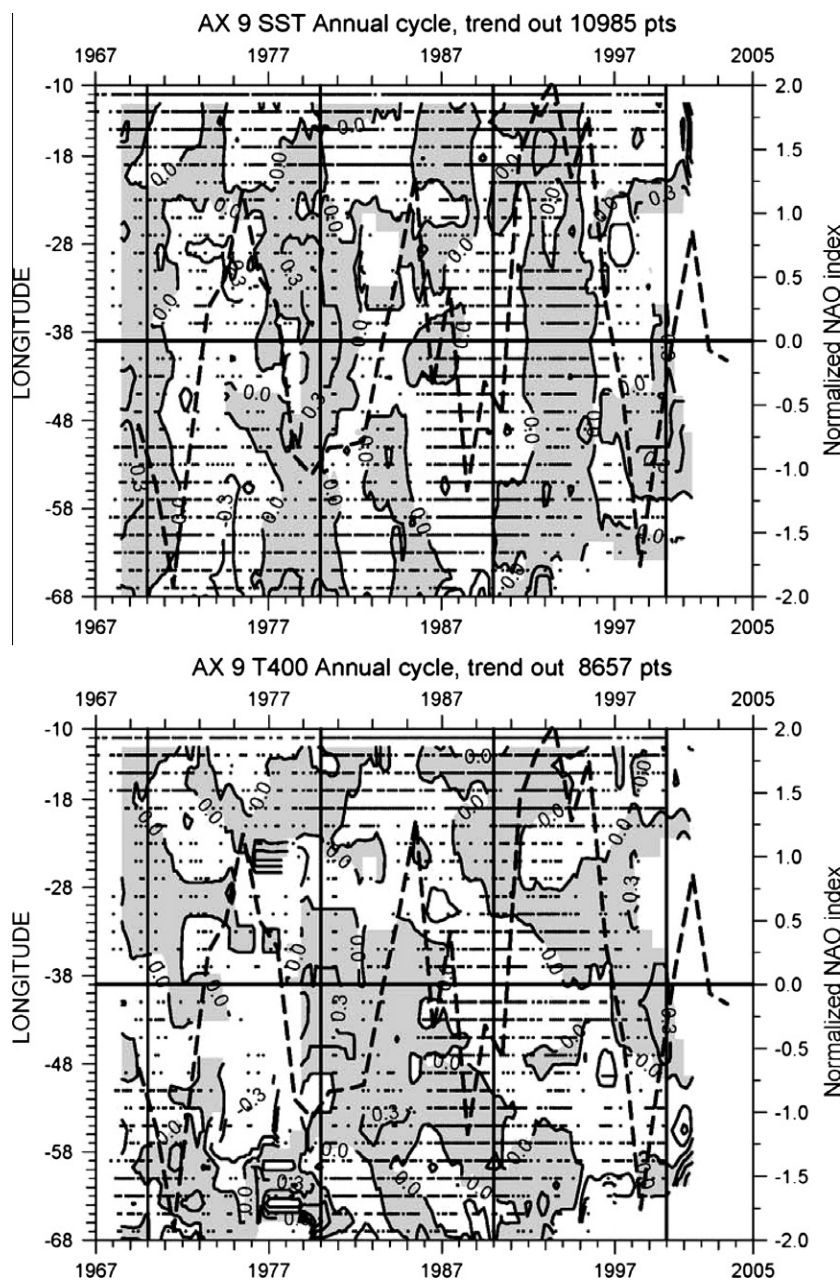


Fig. 12. Same as Fig. 4, except for AX9 and contour interval 0.3 °C for both panels.

Throughout the entire record in this latitudinal band there is no obvious correlation with the NAO.

3.2.5. AX6 and AX8

Both AX6 and AX8 extend from New York to the Gulf of Guinea (Fig. 1). They cross the GS, STG and North Equatorial Current with the same overall mean temperature structure along these sections (not shown) as observed along AX10. Similarly the SST and T400 time series exhibit comparable anomaly patterns to those observed along AX10 (not shown). The sections thus provide minimal additional information on the mean properties or variability of the features crossed by AX10 and will not be discussed further except for a portion of AX6 in a later section.

3.2.6. AX7

This transect crosses the Atlantic from Miami to the Mediterranean, passing through the STG (Fig. 1). AX7 begins in the Straits of Florida where the Florida Current appears as an eastward deepening of the average isotherms (Fig. 10). AX7 then crosses the Antilles Current. The isotherm slopes indicate opposing geostrophic shear above and below 400 m but the surface flow is northward along the western boundary (Fig. 1).

The eastward Subtropical Counter Current is located between 27°N and 29°N from about 75°W to 60°W. This eastward flow is not as apparent in the subsampled currents of Fig. 1 as when all the currents are plotted (not shown). AX7 traverses along the current, thus there is no obvious isotherm slope associated with this flow. The center of the STG along AX7 is located between about 77°W and 73°W (Fig. 10). The weak vertical temperature gradients indicative of 18 °C Water are observed from about 75°W to the crest of the MAR at 41°W.

Fratantoni (2001) shows a schematic location for the Azores Current at 34°N between 44°W and 27°W similar to the location in Fig. 1. Thus, AX7 is traversing along this flow and isotherms slopes (Fig. 10) are not dramatic in this region of eastward flow (Fig. 1). The shoaling isotherms on the eastern end of AX7 are indicative of the Canary Current. Variability along AX7 will be described in Section 4.

3.2.7. AX5 and AX9

AX5 extends from the southwestern corner of Great Britain to the Panama Canal (Fig. 1). AX5 thus crosses AX6, AX7 and AX10. The signals in AX5 (not shown) have been reviewed and the information relative to major features is similar to that found in the other 3 sections. Thus, no additional consideration of this section will be given.

East of the Antillean Arc beginning at about 58°W to the crest of the MAR at about 47°W, AX9 isotherms slope in opposite directions above and below 100 m (Fig. 11). Total surface currents shown in Fig. 1 indicate that AX9 is crossing a region of northward flow (i.e., the deeper slopes below 100 m are controlling the surface flow). East of the MAR, isotherm slope is representative of the North Equatorial Current consistent with the drifter-derived currents given in Fig. 1.

The SST TDP (Fig. 12) displays primarily section-long anomalies of the same sign. There is no suggestion of either signal propagation or obvious correlation between the SST anomalies and the NAO. After approximately 1980 and prior to 2000, T400 anomalies display a westward movement (Fig. 12). Thus, there is a difference in the two anomaly patterns deserving additional study. The T400 variability will be addressed in more detail in Section 4.

3.2.8. AX11 and AX12

Both sections traverse the extreme eastern subtropical NA (Fig. 1). AX12 crosses the upwelling regions off the west coast of Africa. Temperature characteristics along this line will be addressed.

From 40°N to about 26°N, AX12 is located on the extreme eastern side of the STG. The mean isotherm slopes (Fig. 13) and surface currents (Fig. 1) indicate that the flow is to the southwest in this band. From 20°N to 26°N, isotherm slope is indicative of eastward geostrophic shear. However, the total surface currents remain to the west in this band (Fig. 1). AX12 is crossing an upwelling zone here and the isotherm slope is most likely indicative of this feature.

In the 40–26°N band, same-signed SST anomalies extend across the entire latitude range with a quasi-decadal signal (Fig. 14). These SST anomalies are also in-phase with the NAO, suggestive of local surface flux forcing (i.e., positive NAO anomalies with

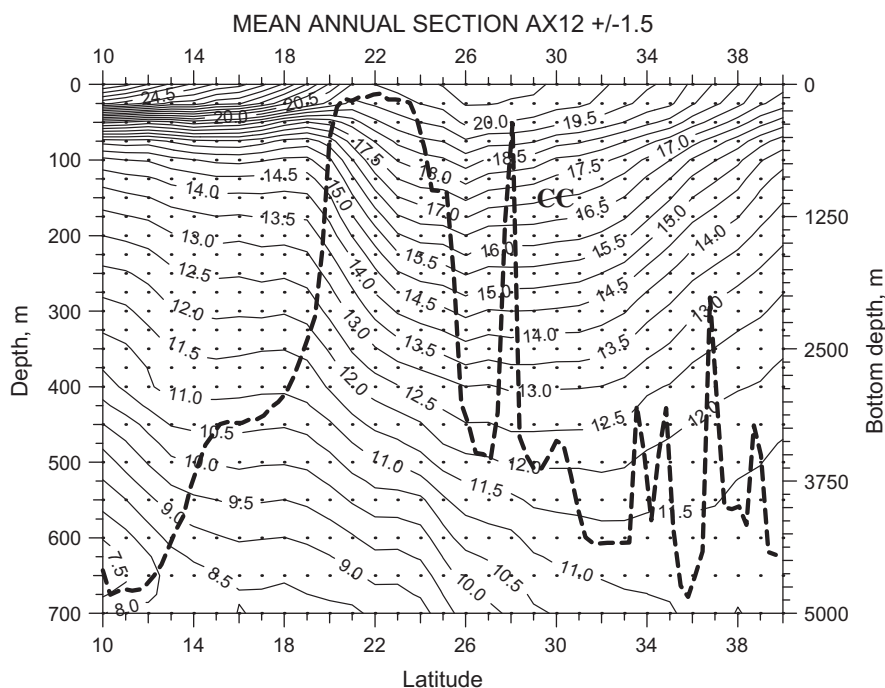


Fig. 13. Same as Fig. 3, except for AX12 and CC = Canary Current.

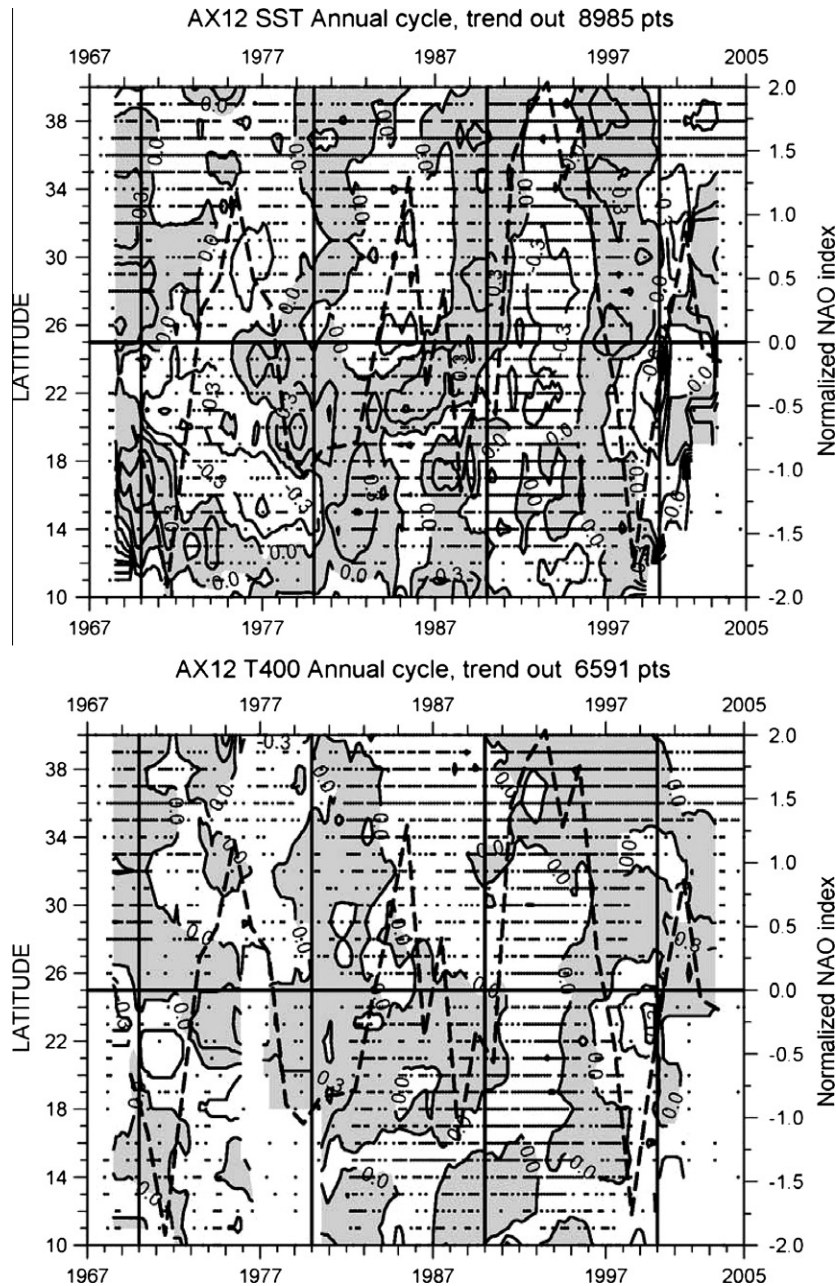


Fig. 14. Same as Fig. 4, except for AX12 and contour interval 0.3 °C for both panels.

associated stronger winds and surface fluxes generate negative SST anomalies). In the upwelling band, approximately 20–26°N, from approximately 1968 through 1976 a period of increased upwelling is followed by a 1977 through 1989 period of decreased upwelling. Both periods, in this latitudinal band include first a minimum in NAO index followed by a maximum (Fig. 14).

4. Discussion

The variability captured in the long-term LD section records will now be illustrated through several examples around the NA basin.

4.1. Subpolar gyre

Based on results from an ocean general circulation model, Lohmann et al. (2009) hypothesize that the ocean was preconditioned

by the 1989–1995 period of positive NAO (not as apparent in Fig. 4 as the trend has been removed) and in combination with a sudden drop in the NAO in 1995/1996 led to the weakening of the SPG. R99 reach a similar conclusion based on AX2 data.

Alternatively, both Häkkinen and Rhines (2009) and Lozier and Stewart (2008) attribute the change in eastern Atlantic SST in the mid-1990s (Fig. 4) to a change in source waters to the region. Häkkinen and Rhines (2009) attribute the change in SST to an increased northeastward flow of warm STG waters to the SPG. Fratantoni (2001) suggested a similar change in circulation associated with the NAO event.

Lozier and Stewart (2008) attribute the changes in the properties of waters entering the Rockall Trough to movements of the subpolar front and associated changes in the amount of Mediterranean Sea outflow moving north. They hypothesize that during periods of high NAO index, the subpolar front moves eastward constricting warm salty northward flow of Mediterranean Sea outflow

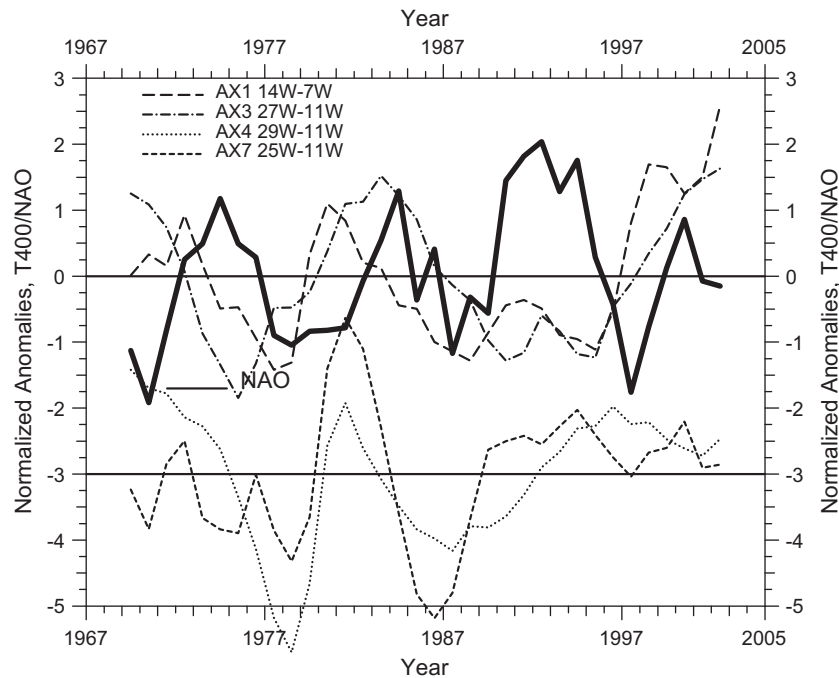


Fig. 15. Normalized by record length standard deviation time series of the NAO and eastern Atlantic T400 anomalies ($^{\circ}\text{C}$) for the longitudinal bands of the LD transects shown in Fig. 1 and noted on the figure.

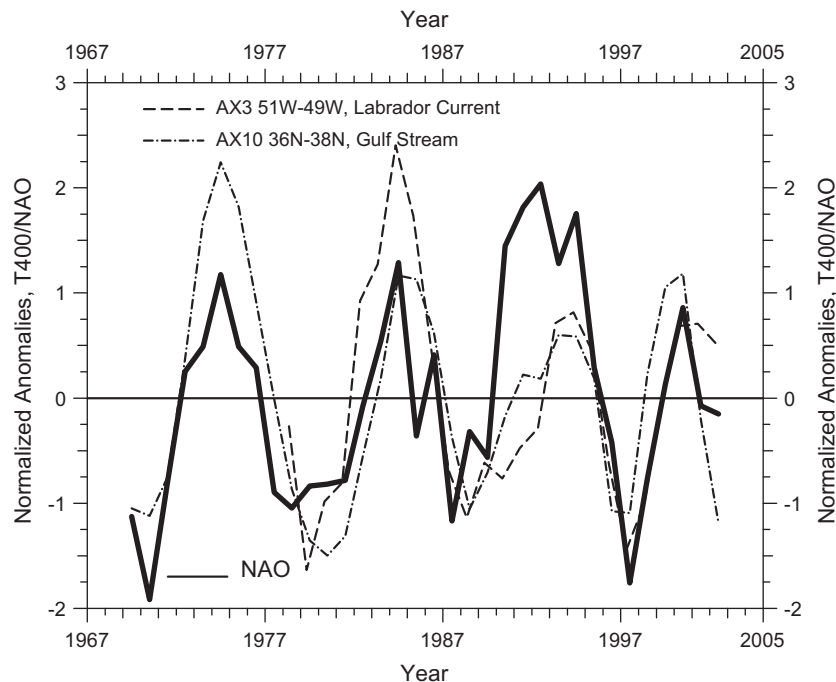


Fig. 16. Normalized by record length standard deviation time series of the NAO and SST for longitudinal bands including the Labrador Current crossing AX3 and the Gulf Stream crossing AX10 (see Fig. 1 for transect and current locations).

along the eastern boundary, with opposite conditions occurring during low NAO index. Obviously, the two explanations are not mutually exclusive.

AX1 is located north of 55°W in the SPG (Fig. 1). In the eastern Atlantic, AX3 is located north of 40°N on the boundary separating northward flow from southward flow. The eastern ends of AX4 and AX7 are located in the Canary Current of the STG. Individual T400 time series have been generated for longitudinal bands located on the eastern ends of these four transects (Fig. 15).

The temperature data from these sections cannot distinguish between water masses implied by the Häkkinen and Rhines (2009) and Lozier and Stewart (2008) hypotheses. However, T400 records can differentiate between colder SPG and/or less Mediterranean water masses from warmer STG and/or more Mediterranean water masses along the boundary. In both AX1 and AX3 time series from the late-1980s to the mid-1990s T400 anomalies are mostly negative and the NAO index positive (Fig. 15). These anomalies are consistent with both the Häkkinen and Rhines (2009) and Lozier and Stewart (2008) proposals for a predominantly

SPG source by the former authors and a reduced Mediterranean source by the latter.

After 1996 the AX1 and AX3 T400 anomalies (Fig. 15) have changed signs consistent with a more subtropical source of transport to the SPG, Häkkinen and Rhines (2009), and/or an increased Mediterranean source of water masses, Lozier and Stewart (2008). Thus both hypotheses are supported by the T400 time series and suggest that ocean circulation also plays a role in the SPG weakening.

Häkkinen and Rhines (2009) attribute the change in source waters to the eastern boundary to a change in NAO sign from positive to negative and the effect of this change on the wind stress curl. They go on to note that because of their short observational record (i.e., drifters) they cannot determine if this transition is part of a longer-term trend or a decadal signal. However, the longer AX3 XBT record (Fig. 7) suggests that the observed changes are periodic rather than sporadic.

The time series in the Canary Current, AX4 and AX7, are in-phase with those from the northern sections at the beginning of the time series but are out of phase beginning in the early 1980s (Fig. 15). There is no consistent phase relation between these records and the NAO time series. Thus, additional study is required to determine the relation of this portion of the eastern STG and the NAO.

4.2. Labrador Current and Gulf Stream

Rosby and Benway (2000) find evidence that changes in the position of the Gulf Stream “may be governed by a time-varying outflow of waters from the Labrador Shelf regions”. AX3 crosses the Labrador Current and AX10 crosses the GS at distinctly different longitudes (Fig. 1). An AX3 T400 time series in the longitudinal band that crosses the Labrador Current, 51–49°W, (Fig. 7) can only be generated post 1980. Thus, an AX3 Labrador Current time series representing this flow is started in 1980 for comparison with the longer GS T400 record at AX10.

The Labrador Current T400, GS T400 and NAO time series are in-phase throughout the period of overlap, Fig. 16. The current crossings at AX3 and AX10 are separated by approximately 20 degrees of longitude. Negative T400 anomalies are consistent with increased transport of colder waters by the Labrador Current as it moves around and across the Tail of the Grand Banks crossing AX3 (Fig. 1). Negative T400 GS anomalies are indicative of southward migrations of the current. Thus, over the 20-year record, increased southward transport by the Labrador Current could be responsible for southward GS migrations. Alternatively, Peña-Molino and Joyce (2008) argue for a similar relation between the intensity of the DWBC and the GS as the former passes under the latter leaving the continental shelf.

4.3. Subtropical gyre

Decadal signals have been found in observations of (e.g., Molinari et al., 1997) and numerical model results (e.g., Ezer, 1999) from the NA STG. Largest amplitudes are primarily found at the depths of the thermocline in these studies. AX6, AX7 and AX10 all traverse the central-western portion of the STG (Fig. 1) and T400 time series have been constructed from the portions of these sections located in the gyre (Fig. 17).

Prior to 1992, the three records are essentially in-phase exhibiting a quasi-decadal signal (Fig. 17). After 1992, the AX6 and AX7 records remain somewhat in-phase but the AX10 series becomes out of phase with the former transects, possibly because of spatial differences in either their locations (Fig. 1) and/or the structure of STG variability. When the three records are in-phase, there is the suggestion that extremes in the NAO index, either positive or negative lead to similarly signed extremes in T400 (Fig. 17). Such an in-phase relation is obviously not consistent with local air–sea forcing of upper 400 m temperature anomalies (i.e., positive NAO, lower temperatures).

Sturges and Hong (1995), Groetzner et al. (1998) and Ezer (1999), for example, find that westward propagating planetary

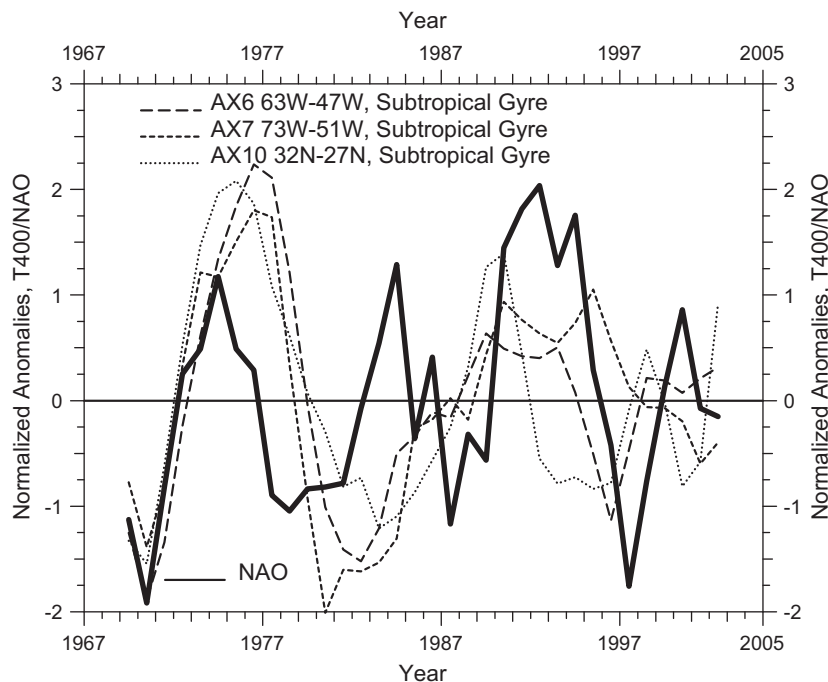


Fig. 17. Normalized by record length standard deviation time series of the NAO and T400 sections crossing the subtropical gyre within the longitudinal swaths noted on the figure.

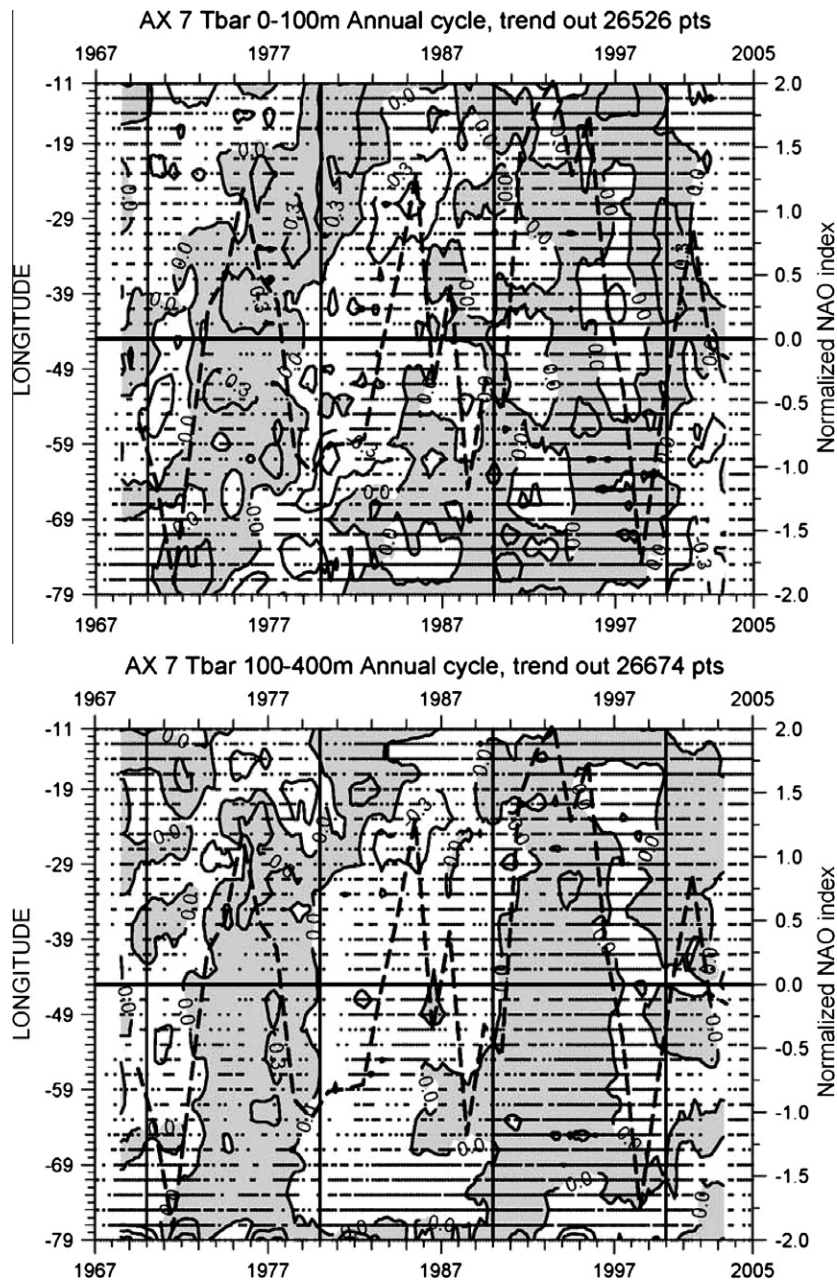


Fig. 18. Upper panel: Time-distance plot of the average temperature ($^{\circ}\text{C}$) between the sea surface and 100 m along AX7. Lower panel: Same as upper panel except for the averaging depth interval, 100–400 m.

waves and/or gyre currents are responsible for the transition from one phase of the decadal cycle to another in the STG at mid latitudes. Watanabe et al. (1999) use all temperature data collected between 1950 and 1992 in the gyre, thus including uncorrected XBT data. They averaged the data onto a 5° grid and filtered the resulting time series with a 5–20 year band pass filter.

They observe that along 32.5°N observed anomalies of the depth-averaged temperature of the upper 100 m propagate eastward in contrast to the westward propagation in their model. However, the observational record is noisy and the propagation signal is weak. There is stronger visual evidence for westward propagation of observed temperature anomalies in their 100–500 m layer (i.e., the thermocline) after 1960. Their model results as well as those of others such as Groetzner et al. (1998), for instance, simulate westward propagation of temperature anomalies for the entire surface layer.

Similar layer calculations were computed from data collected along AX7, which is close to 32.5°N , particularly in the central and eastern Atlantic (Fig. 1). Prior to 1990, there is eastward propagation of temperature anomalies in the 0–100 m layer (Fig. 18). After 1990, no indication of propagation is evident. There is also no obvious correlation between the temperature anomalies and the NAO.

Because of the paucity of data below 400 m, a similar calculation to that of Watanabe et al. (1999) was performed with 400 m as the bottom depth. In the deeper 100–400 m layer there is also no indication of propagation in either direction (Fig. 18). Most same-signed anomaly events extend across the entire basin. There is neither an obvious periodicity in the time series nor similar timing of extreme events in the NAO or temperature records.

Along AX9 westward propagation of T400 anomalies is observed (Fig. 12). However, this section is considerably farther south

than those considered by Sturges and Hong (1995) and Watanabe et al. (1999). In addition AX12, outside the coastal upwelling region, shows a correlation between SST anomalies and the NAO (Fig. 14). Thus, the decadal mechanism of STG currents transporting SST anomalies from the eastern Atlantic to cause phase changes in quasi-decadal signals in the western gyre as proposed by Groetzner et al. (1998), for example, can not yet be discounted.

5. Recommendations

(1) Perform similar studies of information content on other LD lines. (2) Determine if information content is affected by data not only collected along specific lines but as in the 1970s and 1980s from data taken from other nearby (i.e., within the 3° swath) lines or cruises. (3) Perform studies to determine if the Argo network and/or satellite altimetry can supply information equivalent to that provided in LD transects. (4) If a line is no longer operating in LD mode but is active in high-density mode determine if the reduced temporal resolution available from HD sampling provides comparable information to the LD section. (5) Encourage operational agencies to ensure that all the required meta-data accompany XBT profiles submitted to national and international data repositories. (6) Continue studies of FRE and temperature biases in XBT data to develop community-wide accepted corrections that provide climate quality data. (7) Implement the following recommendations relative to data collection along the lines discussed in the text. Status of the lines during 2009 is given as well as the rationale for recommended action.

AX1: Continue in LD mode. Line crosses several currents that provide sources for water masses that undergo transformation farther north to become components of NADW and other current bringing NADW south.

AX2: Line no longer active, restart in LD mode based on the same rationale as for AX1.

AX3: Active in high-density mode, restart in LD mode as the transect crosses the GS, Labrador Current and NAC, all of which contribute to NADW. In the east AX3 provides a record of changes in temperature properties to Nordic Seas.

AX4: Line no longer active. Provides information very similar to AX3.

AX5: Line no longer active. Crosses AX4, AX7 and AX10 providing similar information as these transects.

AX6: Line no longer active. Crosses AX4, AX7 and AX9 providing similar information as these transects.

AX7: Active in high-density mode. Determine if similar time dependent signals found in LD mode are resolved. Bisects subtropical gyre and provides information on eastern boundary conditions. Combined with AX10 provides a basin wide characterization of the STG.

AX8: Active in frequently repeated mode. Tropical and South Atlantic characteristics should be addressed in another paper.

AX9: Line no longer active. Restart as it provides information on southern boundary of STG and eastern boundary.

AX10: Active in high-density mode. Determine if similar time dependent signals found in LD mode are resolved. Provides information on Slope Current, GS, STG and North Equatorial Current. Combined with AX7 provides a basin wide characterization of the STG.

AX11: Active in frequently repeated mode, continue because of difficulty in restarting lines in region traversed.

AX12: Line no longer active. Restart as it provides information on eastern boundary (e.g., upwelling off Senegal).

AX29: Line no longer active. Tropical and South Atlantic characteristics along transect should be addressed in another paper.

AX32: Active in low-density mode. Continue because of additional instrumentation onboard vessel providing data not available from XBTs alone (Rossby and Gottlieb, 1998).

Acknowledgements

NOAA's Climate Project Office and the Physical Oceanography Division (PhOD) of NOAA's AOML funded this work. Neither group participated in the preparation of this manuscript. The financial support provided by PhOD, the programming support provided by Mr. J. Festa, and the figure preparation by Mrs. R. Lusic are gratefully acknowledged. The excellent comments provided by Dr. C. Meinen and three anonymous reviewers are also greatly appreciated.

Appendix A. Acronym list: Complete citations are given in the list of references

BT08 = Brambilla and Talley (2008)
 CTD = conductivity temperature depth
 F03 = Flatau et al. (2003)
 FR = frequently repeated
 FRE = Fall Rate Equation
 H95 = Hanawa et al. (1995)
 HD = High density
 LD = Low density
 NA = North Atlantic
 NADW = North Atlantic Deep Water
 NAO = North Atlantic Oscillation
 NOAA = National Oceanic and Atmospheric Administration
 NODC = National Oceanographic Data Center
 PhOD = Physical Oceanography Division
 R99 = Reverdin et al. (1999)
 SST = sea-surface temperature
 SPG = subpolar gyre
 STG = subtropical gyre
 T400 = depth-averaged temperature of the upper 400 m
 TDP = time-distance plot
 TOGA = Tropical Ocean Global Atmosphere
 WOCE = World Ocean Circulation Experiment
 XBT = expendable bathythermograph

References

- Baringer, M.O., Garzoli, S.L., 2007. Meridional heat transport determined with expendable bathythermographs, Part I: error estimates from model and hydrographic data. *Deep-Sea Res. Part 1* 54, 1390–1401.
- Brambilla, E., Talley, L., 2008. Subpolar Mode Water in the northeastern Atlantic: 1. Averaged properties and mean circulation. *J. Geophys. Res.* 113. doi:10.1029/2006JC004062.
- Domingues, C.M., Church, J.A., White, N.J., Gleckler, P.J., Wijffels, S.E., Barker, P.M., Dunn, J.R., 2008. Improved estimates of upper-ocean warming and multi-decadal sea-level rise. *Nature* 453, 1090–1093.
- Ezer, T., 1999. Decadal variabilities of the upper layers of the subtropical North Atlantic; an ocean model study. *J. Phys. Oceanogr.* 12, 3111–3124.
- Flatau, M.K., Talley, L., Niiler, P.P., 2003. The North Atlantic Oscillation, surface current velocities and SST changes in the Subpolar North Atlantic. *J. Climate* 16, 2355–2369.
- Fratantoni, D.M., 2001. North Atlantic surface circulation during the 1990s observed with satellite-racked drifters. *J. Geophys. Res.* 106, 22067–22093.
- Gould, J. et al., 2004. Argo profiling floats bring new era of in situ ocean observations. *EOS, Trans. Am. Geophys. Union* 85, 185.
- Gouretski, V., Koltermann, K.P., 2007. How much is the ocean really warming? *Geophys. Res. Lett.* 34, L01610. doi:10.1029/2006GL027834.
- Greene, C.H., Pershing, A.J., 2003. The flip-side of the North Atlantic Oscillation and modal shifts in slope-water circulation patterns. *Limnol. Oceanogr.* 48, 319–322.
- Groetzner, C., Latif, M., Barnett, T., 1998. A decadal climate cycle in the North Atlantic as simulated by the ECHO coupled model. *J. Climate* 11, 831–847.
- Häkkinen, S., Rhines, P.B., 2004. Decline of subpolar North Atlantic circulation during the 1990s. *Science* 304, 555–559.

- Häkkinen, S., Rhines, P.B., 2009. Shifting surface currents in the northern North Atlantic Ocean. *J. Geophys. Res.* 114. doi:10.1029/2008JC004883.
- Halliwel, G.R., Peng, G., Olson, D.B., 1994. Stability of the Sargasso Sea subtropical frontal zone. *J. Phys. Oceanogr.* 24, 1166–1183.
- Hanawa, K., Rual, P., Bailey, R., Sy, A., Szabados, M., 1995. A new depth-time equation for Sippican or TSK T-7, T-6 and T-4 expendable bathythermographs (XBT). *Deep-Sea Res.* 42, 1423–1451.
- Hurrell, J.W., 1995. Decadal trends in the North Atlantic Oscillation, regional temperature and precipitation. *Science* 269, 676–679.
- Hurrell, J.W., Kushnir, Y., Ottersen, G., Visbeck, M., 2003. An overview of the North Atlantic Oscillation. *Am. Geophys. Union Geophys. Mono.* 138, 1–36.
- Ishii, M., Kimoto, M., 2009. Reevaluation of historical ocean heat content variations with time-varying XBT and MBT depth bias corrections. *J. Oceanogr.* 65, 287–299.
- Joyce, T.M., Deser, C., Spall, M.A., 2000. The relation between decadal variability of subtropical mode water and the North Atlantic Oscillation. *J. Climate* 13, 2550–2569.
- Krauss, W., 1995. Currents and mixing in the Irminger Sea and in the Iceland Basin. *J. Geophys. Res.* 100, 10851–10871.
- Levitus, S., Antonov, J.I., Boyer, T.P., Locarnini, R.A., Garcia, H.E., Mishonov, A.V., 2009. Global ocean heat content 1955–2008 in light of recently revealed instrumentation problems. *Geophys. Res. Lett.*, 36. doi:10.1029/2008GL037155.
- Lohmann, K., Drange, H., Bentsen, M., 2009. A possible mechanism for the strong weakening of the North Atlantic subpolar gyre in the mid-1990s. *Geophys. Res. Lett.*, 36. doi:10.1029/2009GL039166.
- Lozier, M.S., Stewart, N.M., 2008. On the temporally varying northward penetration of Mediterranean Overflow Water and eastward penetration of Labrador Sea Water. *J. Phys. Oceanogr.* 38, 2097–2103.
- Lumpkin, R., Garraffo, Z., 2005. Evaluating the decomposition of tropical Atlantic Drifter Observations. *J. Atmos. Oceanic Technol.* 22, 1403–1415.
- Molinari, R.L., 2004. Annual and decadal variability in the western subtropical North Atlantic: signal characteristics and sampling methodologies. *Prog. Oceanogr.* 62, 33–66.
- Molinari, R.L., Mayer, D.A., Festa, J.F., Bezdek, H.F., 1997. Multiyear variability in the near-surface temperature structure of the midlatitude western North Atlantic Ocean. *J. Geophys. Res.* 102, 3267–3278.
- Peña-Molino, B., Joyce, T.M., 2008. Variability in slope Water and its relation to the Gulf Stream path. *Geophys. Res. Lett.* 35. doi:10.1029/2007/GL032183.
- Phillips, H.E., Joyce, T.M., 2007. Bermuda's tale of two time series: hydrostation S and BATS. *J. Phys. Oceanogr.* 37, 554–571.
- Pickart, R.S., Torres, D.J., Fratantoni, P.S., 2005. The east Greenland spill jet. *J. Phys. Oceanogr.* 35, 1037–1053.
- Reverdin, G., Verbrugge, N., Valdimarsson, H., 1999. Upper ocean variability between Iceland and Newfoundland, 1993–1998. *J. Geophys. Res.* 104, 29599–29611.
- Rosby, T., Benway, R.L., 2000. Slow variations in mean path of the Gulf Stream east of Cape Hatteras. *Geophys. Res. Lett.* 27, 117–120.
- Rosby, T., Gottlieb, E., 1998. The Oleander project: monitoring the variability of the Gulf Stream and adjacent waters between New Jersey and Bermuda. *Bull. Am. Meteorol. Soc.* 79, 5–18.
- Sippican, 1983. Operation/Maintenance Manual MK-9 Digital XBT/XSV System. R-1197/B. Sippican (now Lockheed Martin Sippican). Ocean Systems Inc., Marion, Massachusetts.
- Smith, N. et al., 1999. The role of XBT sampling in the ocean thermal network. In: Smith, N., Koblinsky, C. (Eds.), *Proceedings The Ocean Observing System for Climate, OCEANOBS 99*. Saint-Raphael, France.
- Stommel, H., Niiler, P., Anati, D., 1978. Dynam9c topography and recirculation of the North Atlantic. *J. Mar. Res.* 36, 449–468.
- Sturges, W., Hong, B.B., 1995. Wind forcing of the Atlantic thermocline along 32N at low frequencies. *J. Phys. Oceanogr.* 25, 1706–1715.
- Tsuchiya, M., 1985. Evidence of a double-cell subtropical gyre in the South Atlantic Ocean. *J. Mar. Res.* 43, 57–65.
- Visbeck, M., Chassignet, E.P., Curry, R.G., Delworth, T.L., Dickson, R.R., Krahnemann, G., 2003. The ocean's response to North Atlantic Oscillation variability. *Am. Geophys. Union Geophys. Mono.* 138, 113–146.
- Wallace, J.M., Gutzler, D.S., 1981. Teleconnections in the geopotential height field during Northern Hemisphere winter. *Monthly Weather Rev.* 109, 784–812.
- Watanabe, M., Nitta, T., Kachi, M., 1999. A comparison of decadal climate oscillations in the North Atlantic detected in observations and a coupled GC. *J. Climate* 12, 2920–2940.
- Wijffels, S.E., Willis, J., Dominguez, C.M., Barker, P., White, N.J., Gronell, A., Ridgway, K., Church, J.A., 2008. Changing expendable bathythermograph fall rates and their impact on estimates of thermosteric sea level rise. *J. Climate* 21, 5657–5672.